Robotics and Autonomous Systems 58 (2010) 295–305

Contents lists available at ScienceDirect

Robotics and Autonomous Systems

journal homepage: www.elsevier.com/locate/robot

Omnivision-based KLD-Monte Carlo Localization☆

C. Gamallo[a], C.V. Regueiro[b], P. Quintía[b], M. Mucientes[a,*]

[a] *Department of Electronics and Computer Science, University of Santiago de Compostela, E-15782, Spain*

[b] *Department of Electronic and Systems, University of A Coruña, E-15071, Spain*

ARTICLE INFO

Article history:
Available online 20 November 2009

Keywords:
Monte Carlo Localization (MCL)
Omnidirectional camera
Feature-based map

ABSTRACT

Mobile robots operating in real and populated environments usually execute tasks that require accurate knowledge on their position. Monte Carlo Localization (MCL) algorithms have been successfully applied for laser range finders. However, vision-based approaches present several problems with occlusions, real-time operation, and environment modifications. In this article, an omnivision-based MCL algorithm that solves these drawbacks is presented. The algorithm works with a variable number of particles through the use of the Kullback–Leibler divergence (KLD). The measurement model is based on an omnidirectional camera with a fish-eye lens. This model uses a feature-based map of the environment and the feature extraction process makes it robust to occlusions and changes in the environment. Moreover, the algorithm is scalable and works in real-time. Results on tracking, global localization and kidnapped robot problem show the excellent performance of the localization system in a real environment. In addition, experiments under severe and continuous occlusions reflect the ability of the algorithm to localize the robot in crowded environments.

1. Introduction

Nearly all the tasks that an autonomous mobile robot has to carry out require knowledge on the position of the robot. Given a map of the environment, a localization system estimates the pose (position and angle) of the robot in the map based on a motion model of the robot and/or a measurement model for the sensors. A localization algorithm must be reliable, robust and executable in real-time.

Very different types of sensors have been used for localization. In particular, the three most widely used are laser [1,2], sonar [3,4] and cameras [5,6]. In recent years, different successful localization algorithms based on laser range finders have been proposed [7–9].

Moreover, the use of cameras for localization tasks has received increasing attention. The main advantages of these sensors are the quantity and quality of information that can be extracted from one acquisition. This is particularly interesting for localization, as different types of landmarks can be detected using information on shape, color, etc. Popular vision approaches are feature-based and pixel-based. Feature-based techniques [10,11] exploit typical properties of the environment or any distinctive and recognizable objects (landmarks). Pixel-based approaches [5,12] compute the correlation between images, in order to estimate the mobile robot pose.

In real environments, the presence of people in the surrounding of the robot is usual. Both static and moving people are detected by the robot sensors, generating measurements that have to be discarded. These measurements are useless for localization but, also, introduce noise in the localization algorithms, as sometimes measurements coming from people are confused with those from landmarks or other objects used for localization. This problem can be addressed by attempting to classify the measurements coming from people, and those coming from objects that are relevant to the localization task. For example, for laser range finders, several authors have classified measurements in order to distinguish between people and objects [13,14], while others have built maps in the presence of several moving people [15].

Nevertheless, when the environment is highly populated, the problem is not simply that of filtering measurements coming from people, but the inability to sense any landmark over long periods of time, thus rendering localization truly difficult, while the knowledge about the pose has a huge uncertainty. These situations could be typical, for example, for a tour-guide robot operating in a museum, and surrounded by a group of people who are interacting with the robot. The only area of the environment that can be seen regularly in these conditions is the ceiling.

In this article, a localization algorithm for a tour-guide robot operating in a very crowded environment is presented. Due to

☆ This work was supported in part by the Spanish Ministry of Science and Innovation under grant TIN2008-00040. Manuel Mucientes is supported by the *Ramón y Cajal* program of the Spanish Ministry of Science and Innovation.

* Corresponding author.
E-mail addresses: cristina.gamallo@usc.es (C. Gamallo), cvazquez@udc.es (C.V. Regueiro), pquintia@udc.es (P. Quintía), manuel.mucientes@usc.es (M. Mucientes).

0921-8890/$ – see front matter © 2009 Elsevier B.V. All rights reserved.
doi:10.1016/j.robot.2009.08.007

the presence of groups of people, typical localization solutions based on range sensors, such as laser or sonar, or those based on the detection of conventional landmarks with cameras do not work properly. Moreover, the environment cannot be modified by introducing artificial landmarks to facilitate localization.

Our approach is based on a map of the lights (landmarks) placed on the ceiling of the environment. These landmarks are easy to detect, repetitive and usually visible for long trajectories. On the other hand, most buildings have these kinds of landmarks, so there is no need for prior adaptation of the environment in order to use the proposed localization method. The main problem is their individual identification, as they are usually identical, making the data association more difficult. Measurements from the environment are acquired with an omnidirectional camera fitted with a fish-eye lens. This sensor provides an extremely wide field of vision, covering half the space of the environment and, therefore, it can get a high amount of information in one acquisition.

In recent years, probabilistic techniques have been successfully applied in different fields of robotics, such as mapping, localization, tracking, or planning [16]. The application of particle filters for localization, named Monte Carlo Localization (MCL), has proved to be a very popular approach for solving both position tracking and global localization problems. The proposed localization algorithm is based on MCL, combined with the injection of random particles to recover from failures (kidnapped robot problem), and with an efficient implementation due to the adaptive sample set size through KLD-sampling.

In summary, the main points of our proposal are: first, the localization algorithm, KLD-Augmented-MCL, can recover from failures, works in real-time and is robust to severe and continuous occlusions. In second place, data of the landmarks in the environment are obtained with an omnidirectional camera with a fish-eye lens and an algorithm for the detection of the lights on the ceiling. Finally, the system has been tested in real and complex conditions, showing a good performance.

The article is organized as follows. Section 2 analyzes other contributions for localization, in particular for vision-based approaches. Section 3 describes the localization algorithm (KLD-Augmented-MCL), while Section 4 presents the measurement model. Finally, Section 5 shows the results for different experiments in real conditions, and Section 6 points out the conclusions.

2. Related work

There has been extensive research in the literature to solve the localization problem using vision. Most of the algorithms are based on probabilistic approaches. For example, in [17], a localization system based on the MCL algorithm is presented. This algorithm is a Bayesian filtering method that uses a sampling-based density representation. The robot was equipped with a monocular camera pointing to the ceiling, and the map was built as a mosaic of 250 images captured and globally aligned. The pose of the robot was estimated using information of the brightness of the images, and tests of tracking and global localization were performed. A similar approach has also been followed in [1].

In [18], a localization system using a particle filter and a monocular camera was presented. The Scale-Invariant Feature Transform (SIFT) signature of the images in a database was used for comparison with the present image. The majority of vision-based approaches rely on the existence of a database of images that are compared with the present image. This has several disadvantages. In first place, the images are recorded for a route, and if the route is changed, or the robot has a very different orientation in a position, the error in the localization increases. In second place, the localization error increases greatly owing to partial occlusions, for example in the presence of people. Finally, this kind of algorithm is highly sensitive to modifications in the environment (e.g. a door was closed and now is open, a new object is placed or removed from the environment, etc.).

Stereo camera systems have also been used for localization, as in [19] with an MCL algorithm. Images were recorded on a database and compared with the present one using a histogram of local features. The system was tested on tracking, global localization and kidnapping problems.

Omnidirectional cameras are particularly interesting for localization algorithms due to their high field of view (FOV). The first work combining localization and omnivision was published in [20]. In [21], authors proposed a hierarchical (three-step) algorithm that used line descriptors, a global filter (based on color descriptors) and a pyramid matching kernel. In [22], the similarities between images were measured using the average color value of each sector of the image, while in [23] the measurement model used the gray level curve sectors, and a sector matching algorithm based on the Dempster–Shafer fusion of different criteria.

Many omnivision approaches are based on the MCL algorithm using different techniques for the estimation of the weights of the particles. For example, in [12], the measurement model used the correlation of the present image with a set of images that had been recorded for a specific route. That comparison was carried out with a modified version of the SIFT algorithm. The system can cope with partial occlusions, but increasing the localization error (4 m for a 50% occlusion). Another approach was presented in [24], where a Fourier transform of omnidirectional images was used to weight the samples. In [6], the chromatic transitions for scan matching were employed to estimate the conditional probability of a measurement. Finally, in [25], the system used a graph-based representation of the operation area. The nodes of the graph were labeled with both visual feature vectors (average color value) extracted from omnidirectional images, and odometric data of the robot at the moment of node insertion.

The main differences of our approach with these proposals are:

- We use a feature-based map for localization, as the proposed feature extraction process is able to obtain the landmarks (lights) of the environment. The main advantage of this approach is that the system does not need a database of images and, therefore, the localization algorithm is not limited to certain routes, it is robust to changes in the environment, and also to occlusions, as only a few landmarks of the map are needed for localization at each time instant.
- The proposed algorithm is scalable with the size of the environment, in contrast with those approaches relying on a database of images. Moreover, only a few approaches that use image databases can work in real-time (limiting the size of the database), while our proposal works in real-time with no type of constraint. In addition, the adaptive number of particles contributes to real-time operation.
- Our approach is robust under severe and continuous occlusions, which makes it especially suited to crowded environments.

3. KLD-Augmented-Monte Carlo Localization algorithm

The localization algorithm is based on MCL, i.e. the Probability Density Function (PDF) of the pose of the robot is represented by a set of particles. Each particle is a sample of the PDF, and codifies a possible pose of the robot. Particles are distributed according to the PDF, i.e. the regions of the PDF with a higher probability will have a higher concentration of particles. The basic MCL algorithm (also known as particle filter localization) was proposed in [26,27], and solves both the local and global localization problems. However, the most complex localization problem, the kidnapped robot problem, cannot be solved with the basic MCL.

```
1: static $w_{slow}$, $w_{fast}$, $N_{kld}$
2: $\chi_t = \emptyset$, $\overline{\chi}_{t-1} = \emptyset$, $N_{t-1} = |\chi_{t-1}|$, $N_r = 0$, $N_b = 0$,
   $w_{avg} = 0$
3: for $i = 1$ to $N_{t-1}$ do
4:     if $rand() < \max\left\{0,\ 1 - w_{fast}/w_{slow}\right\}$ then
5:         add random pose to $\overline{\chi}_{t-1}$
6:         $N_r = N_r + 1$
7:     end if
8: end for
9: for all $b \in G$ do
10:     $b = 0$
11: end for
12: $\overline{\chi}_{t-1} = sampler(\chi_{t-1},\ \max\{0,\ N_{kld} - N_r\}) \cup \overline{\chi}_{t-1}$
13: $N_t = |\overline{\chi}_{t-1}|$
14: for $i = 1$ to $N_t$ do
15:     $x_t^i = sampleMotionModel\left(u_t,\ \overline{x}_{t-1}^i\right)$
16:     $w_t^i = measurementModel\left(x_t^i,\ F,\ M\right)$
17:     $\chi_t = \chi_t \cup \left\langle x_t^i,\ w_t^i \right\rangle$
18:     $w_{avg} = w_{avg} + \frac{w_t^i}{N_t}$
19:     if $bin\left(x_t^i\right) = 0$ then
20:         $bin\left(x_t^i\right) = 1$
21:         $N_b = N_b + 1$
22:     end if
23: end for
24: $w_{slow} = w_{slow} + \alpha_{slow}\left(w_{avg} - w_{slow}\right)$
25: $w_{fast} = w_{fast} + \alpha_{fast}\left(w_{avg} - w_{fast}\right)$
26: if $N_b > 1$ then
27:     $N_{kld} = \frac{N_b-1}{2\epsilon}\left\{1 - \frac{2}{9(N_b-1)} + \sqrt{\frac{2}{9(N_b-1)}}z_{1-\delta}\right\}^3$
28: else
29:     $N_{kld} = 1$
30: end if
31: return $\chi_t$
```

Fig. 1. KLD-Augmented-MCL (χ_{t-1}, u_t, F, M).

In a kidnapping situation, the robot is placed in another location while the localization system still believes that the position of the robot is known. Kidnapped robot experiments reflect the ability of the localization algorithm to recover from failures. One approach for solving this problem with the MCL algorithm is the addition of random particles to the particles set. The Augmented-MCL algorithm [8] adds random particles to the set based on the probabilities of sensor measurements. Thus, the lower the average sensor measurements probabilities, the higher the number of random particles added to the set.

In all these MCL algorithms, the number of particles is fixed and must usually be large, in order to represent the PDF in the initial stages of a global localization. However, when the algorithm is simply tracking the position of the robot, the number of particles could be much lower. Therefore, adapting the particles set size improves the efficiency of MCL algorithms. One approach to adapt the number of particles is Kullback–Leibler divergence (KLD) sampling [9]. This is based on the KLD, which measures the difference between two PDFs. KLD-sampling determines the number of samples such that, with probability $1 - \delta$, the error between the true posterior and the sample-based approximation is less than ϵ.

The localization algorithm presented in this article (Fig. 1) is based on the Augmented-MCL algorithm, combined with KLD-sampling. The input parameters of the algorithm are the previous PDF, represented by the particles set (χ_{t-1}), the motion command (u_t), the set of detected features in the present time instant (F), and the map (M). The steps of the algorithm can be classified into three groups:

- *MCL part*: is the core of the algorithm (lines 12–17). It samples the previous particle set, updates the particles using the motion model and, finally, estimates the weight of each particle through the measurement model.
- *Augmented part*: corresponds to the insertion of random particles when the present measurements do not match with the expected ones (lines 3–8, 18, 24 and 25). This allows the algorithm to recover from localization failures, for example in the kidnapping problem.
- *KLD part*: calculates the number of particles that are necessary to appropriately represent the PDF of the pose of the robot (lines 9–11, 19–22, 26–29).

Going into the details, at the beginning of the algorithm (lines 3–8), random particles are added to the particle set: a random number in [0, 1] (*rand* ()) is generated N_{t-1} times (size of χ_{t-1}). Therefore, a random particle is added with probability $\max\{0, 1 - w_{fast}/w_{slow}\}$ to $\overline{\chi}_{t-1}$, which represents the particle set χ_{t-1} after sampling. w_{fast} and w_{slow} are the short- and long-term averages of the measurement likelihoods (weights of the particles). If w_{fast} and w_{slow} are very similar, or $w_{fast} > w_{slow}$, then no random particles will be added. This means that the measurements are the expected ones for the poses represented by the particles. On the other hand, if $w_{fast} < w_{slow}$ the PDF does not correspond with the measurements, and random particles must be added. The lower the quotient between the short and long-term, the higher the number of random particles. For instance, in the kidnapped robot problem w_{fast} decreases drastically, while w_{slow} decreases smoothly and, therefore, the number of randomly generated particles is high in the first iterations after the kidnapping.

In order to derive a statistical bound for the number of particles from the KLD, the state space has to be divided in bins. Lines 9–11 reset the information contained in each bin *b*, storing a value of 0 which indicates that no particles belong to that bin. Next (line 12), the algorithm resamples the initial particle distribution (χ_{t-1}), obtaining $N_{kld} - N_r$ new particles, where N_r is the number of particles randomly generated in the present iteration, and N_{kld} is the statistical bound estimated from the KLD for the particles in the previous iteration. *sampler* () function can be implemented with any sampling algorithm, for example the low variance sampler [16].

The core of the algorithm (lines 14–23) repeats, for each particle in $\overline{\chi}_{t-1}$, the following steps: first, taking into account the previous pose ($\overline{x}_{t-1}^i$) and the motion command (u_t), a random new pose (x_t^i) is drawn according to the motion model. Then, given the new pose, the detected features (F) and the map (M), the measurement model gives the likelihood of the detected features for that pose and map. This likelihood is the weight of the particle (w_t^i). The particle is added to the new set (χ_t), and the average weight is updated (w_{avg}). Finally (lines 19–22), if the bin of the particle is empty, it is set to non-empty and the number of non-empty bins is increased.

Once all the particles have been added to the set, the short- and long-term average weights are updated, using their difference with the present average weight and a parameter (α_{fast}, α_{slow}). These parameters can be considered as decay rates, and they must fulfill that $0 \leq \alpha_{slow} \ll \alpha_{fast}$.

Finally, the statistical bound for the number of particles is calculated (lines 26–29) using the number of non-empty bins (N_b) and the statistical error bounds ϵ and δ. $z_{1-\delta}$ represent the upper $1 - \delta$ quantile of the standard normal distribution. The estimation of the number of particles that are necessary to represent the PDF of the pose of the robot is based on KLD (N_{kld}), and is proportional to the number of non-empty bins (N_b). A high value for N_b means that the particles are distributed over the state space, i.e., there is a high uncertainty in the pose of the robot. Thus, in order to represent that situation and to keep track of all the plausible poses, a higher number of particles is needed. On the other hand, when N_b is low, the particles are concentrated around a few regions of the state space and, therefore, the PDF can also be represented with a lower number of particles.

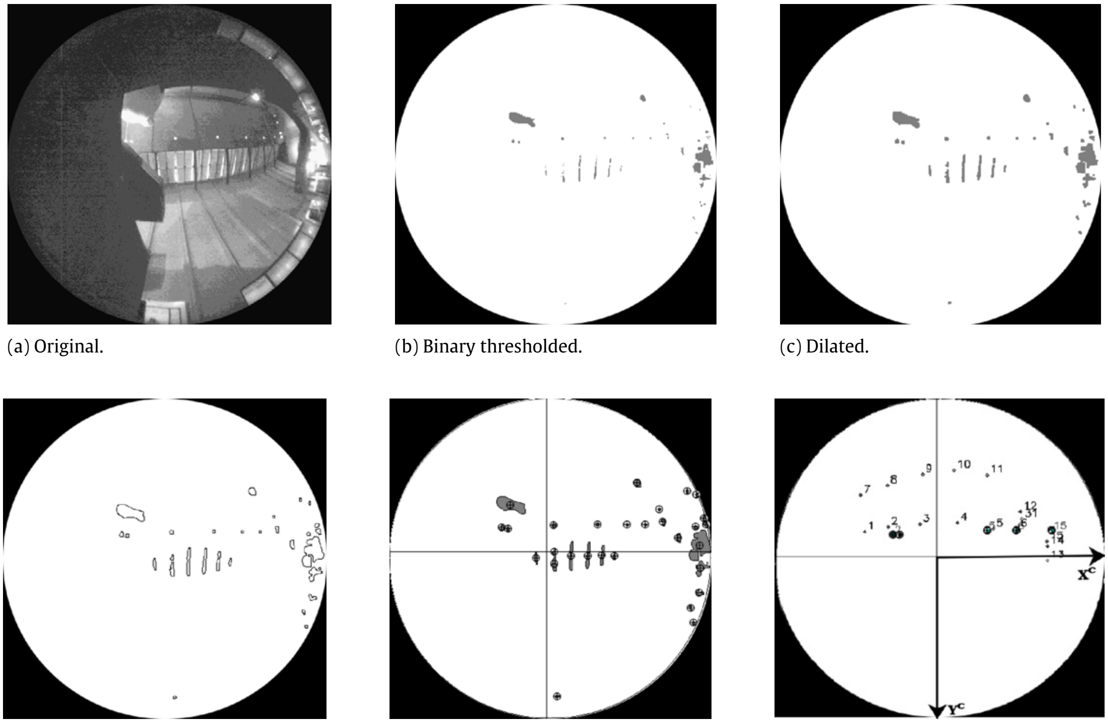

(a) Original.

(b) Binary thresholded.

(c) Dilated.

(d) Edges.

(e) Blobs detection.

(f) Detected features.

Fig. 2. Feature extraction from an omnidirectional image.

One of the factors that can increase uncertainty during localization is the existence of symmetries in the environment. With a fixed number of particles, the set is divided among the different localization hypothesis. The concentration of particles in each cloud could be low and, therefore, the localization can fail due to the elimination of those particles that represent the right pose. On the contrary, through the use of KLD-sampling, the number of particles dynamically increases as the uncertainty in the pose of the robot is high, i.e., there are several good candidate poses due to the symmetries in the environment. Once the robot moves and the ambiguities are solved, uncertainty is reduced and, consequently, the number of particles that are necessary is also lower.

4. Measurement model

The sensor model that has been used is based on feature extraction from the images obtained by an omnidirectional camera with a fish-eye lens. Thus, the localization algorithm relies on a map (M) composed of a set of landmarks. These landmarks are the lights placed on the ceiling of the environment.

4.1. Features extraction

Due to the special characteristics of the landmarks, the feature extraction process can be improved by incorporating a bandpass infrared filter to the camera. The process for features detection consists of five steps: acquisition, preprocessing, segmentation, recognition and features extraction. The output of the system is an array of features for each candidate landmark. In the preprocessing phase, the image (Fig. 2(a)) is transformed to facilitate the processing in the next stages. The techniques that have been used are binary thresholding (Fig. 2(b)) and morphological filtering (dilation) (Fig. 2(c)).

As segmentation techniques, the system uses a Canny filter and contour extraction (Fig. 2(d)). The next step is to extract the characteristics of each region:

- *Perimeter*: number of pixels in the perimeter.
- *Centroid*: coordinates of the center of gravity.
- *Radius*: centroid distance to the center of the image.
- *Azimuth*: orientation of an object in the image with respect to the x-axis.

If a light is pointing directly to the camera, then the acquired image will be saturated (Fig. 3(a)). In such cases, a big blob can be detected and the image has to be processed again using a higher threshold (Fig. 3(b)). This situation can be very frequent when lights are quite close to the camera.

4.2. Camera model

The camera model describes how a 3-dimensional scene is transformed into a 2-dimensional image. The standard model is the *Pin-Hole*, which projects the scene on a flat retina, but it is limited to cameras with FOV $\ll$ 180°. The other cameras require a model based on a spherical retina. In our system, we have used a projection model developed by Pajdla and Bakstein [28] that indicates how a point (B) in a 3-dimensional Cartesian reference system can be transformed to the coordinates of a pixel in a 2-dimensional image. The model requires the calculation of two angles. On one hand, θ (Fig. 4) is the angle formed between the optical axis of the camera and the beam. This beam is the line from the origin of coordinates of the camera to point B. On the other hand, φ is the angle between the x-axis and the projection of the beam on the x–y plane. Next, the distance r (Fig. 4) from the image center (u_0, v_0) to the coordinates of point B in the image (u_B, v_B) is estimated as:

$$r = a * \tan\frac{\theta}{b} + c * \sin\frac{\theta}{d}, \tag{1}$$

where $a, b, c,$ and d are parameters of the model. This function makes it possible to calculate the coordinates of the point in the image (u_B, v_B) depending on the azimuth (φ) and the elevation (θ) (Fig. 4):

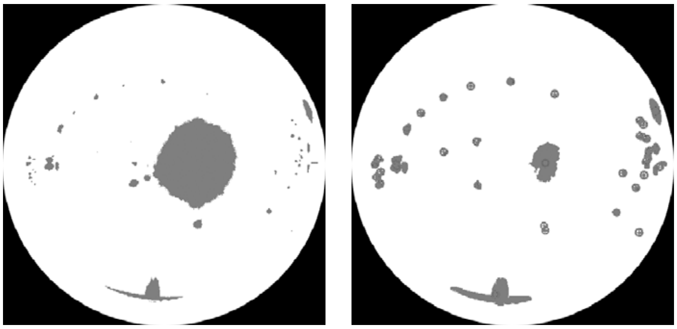

(a) Saturated image.

(b) Postprocessed image.

Fig. 3. Postprocessing phase.

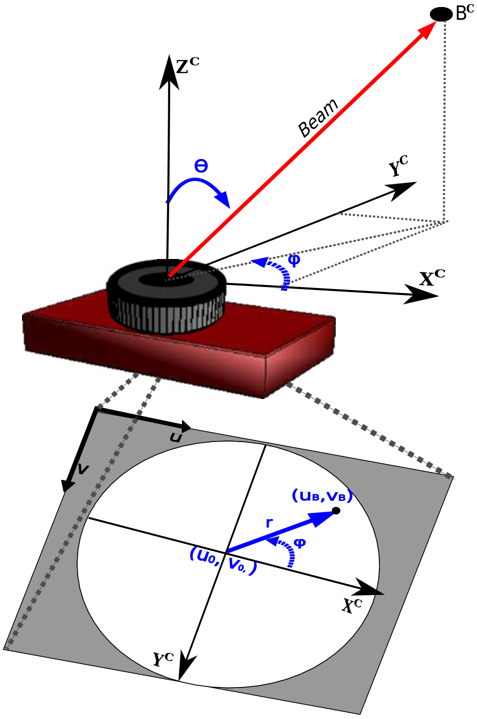

Fig. 4. Projection of a 3-dimensional point B on the image reference system using the omnidirectional camera model.

$$\left.\begin{aligned} u_B &= u_0 + r * \cos\varphi \\ v_B &= \beta * (v_0 + r * \sin\varphi) \end{aligned}\right\} \tag{2}$$

where β is the ratio between the width and the height of a pixel. These equations (Eqs. (1) and (2)) define the omnidirectional camera model.

4.3. Landmark measurements

The map that has been used for localization consists of a list of landmarks, and each landmark is defined by its 3-dimensional coordinates in a Cartesian reference system. As described in Fig. 1 (line 16), given a pose of the robot (x_t), the set of features (F) that have been extracted from an image, and the set of landmarks (M, the map of the environment), the measurement model has to calculate the conditional probability that given the pose and the map, F is the set of detected features at time t. To calculate this probability, we need to have the elements of sets M and F both in the same coordinate system. Therefore, and using the camera model, all the landmarks $B_i \in M$ have to be transformed.

```
$P(F \mid x, M) = 1$
for all $B_i \in M$ do
    $\lambda_i = 0$
end for
for all $F_j \in F$ do
    $P(F_j \mid x, M) = P_{falsePos}$
    for all $B_i \in M$ with $\lambda_i = 0$ do
        $P(F_j \mid x, B_i) =$
            $\max\left\{1 - \frac{\sqrt{\left(u_{F_j} - u_{B_i}\right)^2 + \left(v_{F_j} - v_{B_i}\right)^2}}{max_{dist}}, 0\right\}$
        if $P(F_j \mid x, B_i) > P(F_j \mid x, M)$ then
            $P(F_j \mid x, M) = P(F_j \mid x, B_i)$
        end if
    end for
    $P(F \mid x, M) = P(F \mid x, M) \cdot P(F_j \mid x, M)$
    $\eta = \arg\max_i P(F_j \mid x, B_i)$
    $\lambda_\eta = 1$
end for
return $P(F \mid x, M)$
```

Fig. 5. Maximum likelihood data association.

A landmark projection is the calculation of the pixel coordinates in the image (u_{B_i}, v_{B_i}) for landmark B_i, given its coordinates in the world $(\mathbf{B}_i^W)$ and the coordinates of the camera $(\mathbf{C}^W)$ in the same reference system. First, the landmark coordinates must be transformed from world coordinates $(\mathbf{B}_i^W)$ to the camera reference system $(\mathbf{B}_i^C)$ with the rotation matrix R^C:

$$\mathbf{B}_i^C = R^C \cdot \mathbf{B}_m^W - \mathbf{C}^W. \tag{3}$$

From $\mathbf{B}_i^C$, we obtain the elevation (θ) and the azimuth (φ) angles by applying the traditional Euclidean transformations (Fig. 4). Finally, to obtain the landmark projection $(u_{B_i^C}, v_{B_i^C})$, Eqs. (1) and (2) are applied. The image composed of all the landmark projections is called the map projected image. The measurement model returns the value of the conditional probability $P(F \mid x, M)$. Assuming conditional independence between features, it can be calculated as:

$$P(F \mid x, M) = \prod_j P\left(F_j \mid x, M\right) \tag{4}$$

and, therefore, the probability for each feature F_j can be estimated independently.

In order to calculate the conditional probability, it is necessary to decide the correspondence between each feature F_j and each landmark B_i. This has been solved with the maximum likelihood data association algorithm (Fig. 5). The calculation of $P(F \mid x, M)$

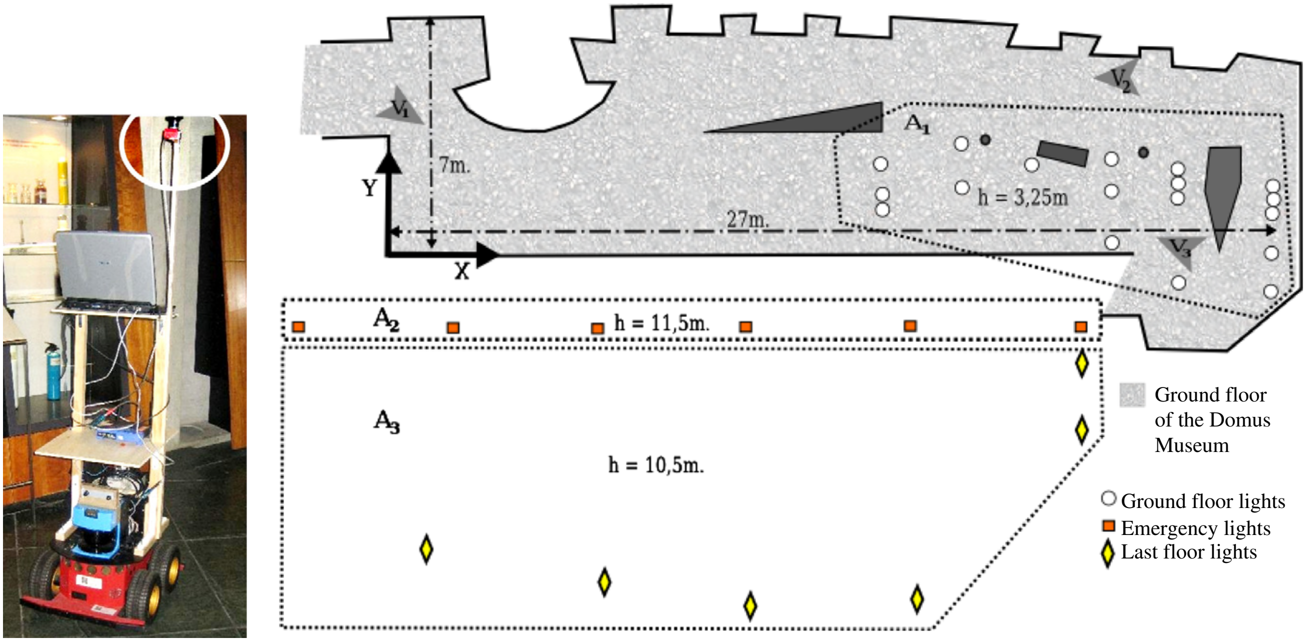

(a) Pioneer 2-AT robot.

(b) Map of the exposition hall.

Fig. 6. Experiments setup.

requires, firstly, the initialization of λ_i for all the landmarks (lines 2–4). This variable indicates whether a landmark B_i has been associated to a feature, and is necessary to avoid the assignment of several features to a landmark. Then, for each feature (line 5), the maximum conditional probability is initialized to $P_{falsePos}$, which is the probability that a feature is not a landmark, but a false positive.

Then, for each landmark (B_i) in the map that has yet to be associated (line 7), the conditional probability of feature F_j given B_i and the pose x is estimated (line 8). In this equation, (u_{F_j}, v_{F_j}) are the coordinates of feature F_j in the image obtained by the camera at the present time instant, (u_{B_i}, v_{B_i}) are the coordinates of landmark B_i in the map projected image, and $\max_{dist}$ is a constant. If the probability is higher than for previous landmarks, then $P\left(F_j \mid x, M\right)$ is updated with this value (lines 9–11). Finally, $P\left(F \mid x, M\right)$ is updated based on Eq. (4) (line 13), and the variable λ_η, where η is the landmark that maximizes the conditional probability $P\left(F_j \mid x, B_i\right)$, is set to 1 (lines 14 and 15). This means that no other features can be associated with that landmark.

5. Results

The localization algorithm has been tested with a *Pioneer* 2-*AT* robot (Fig. 6) equipped with an omnidirectional color digital camera (MDCS2) with a fish-eye lens (FE185C046HA-1, FOV 185°) and a bandpass infrared filter (IRP) type HOYA RT-830. The camera was placed 1.8 m above floor level, in order to minimize the occlusions due to people. Experiments were carried out in an exposition hall (ground floor in Fig. 6(b)) of the Domus Museum (A Coruña, Spain). The environment had a size of 27×7 m^2 and a very uneven floor. The images were obtained at one frame per second during localization, i.e., the robot was moving during the acquisition of the images.

The ground truth was obtained from measurements coming from a laser range finder. Therefore, this ground truth is merely an estimation of the real ground truth. Moreover, it was calculated without the presence of people in the environment, as the information provided by laser range finders is very poor under severe occlusions in very crowded environments. This situation is very typical in the Domus Museum, where the robot is usually completely surrounded by people, even when it is moving.

The map of landmarks used for these experiments consisted of a set of lights placed on the ceiling of the environment. Fig. 6(b) shows the ground floor (where experiments were conducted), and the three different sets of lights that were used for localization: ground floor lights (A_1), emergency lights (A_2), and last floor lights (A_3). The average height of each set of lights is shown is Fig. 6(b) (h value). Fig. 7 shows different snapshots of the environment. The sets of lights have been labeled in these figures. It can be seen that there are several ceilings at different heights and, also, that some lights become occluded from some areas of the environment. Moreover, there are many lights that are not landmarks and, therefore, should be eliminated during the data association process.

Experiments have been designed to prove that the localization algorithm can reliably estimate the pose of a tour-guide mobile robot in different situations (e.g. position tracking, global localization and kidnapped robot problem). Moreover, an analysis on the performance on the algorithm under severe continuous occlusions has been performed. All the experiments have been executed with the following values for the parameters of the algorithm: $\epsilon = 0.20$, $z_{1-\delta} = 0.99$, $\alpha_{slow} = 0.1$, $\alpha_{fast} = 0.5$ and $\max_{dist} = 30$.

5.1. Position tracking

The first set of experiments was carried out to analyze the ability to keep track of the robot's pose, while it was moving in the environment with an average speed of 40 cm/s. Fig. 8 shows the estimated poses and the ground truth for one of these experiments. The black circles are placed every 10 steps.[1] The distance traveled was over 45 m and 110 images were acquired and processed. The poses of two consecutive images had an average distance of 0.4 m, but the change in the pose angle was sometimes quite large. For example, in the middle of the trajectory, the robot turned 180° in three steps.

[1] Each step represents the acquisition of a new image. As has been mentioned, the elapsed time between two steps is one second.

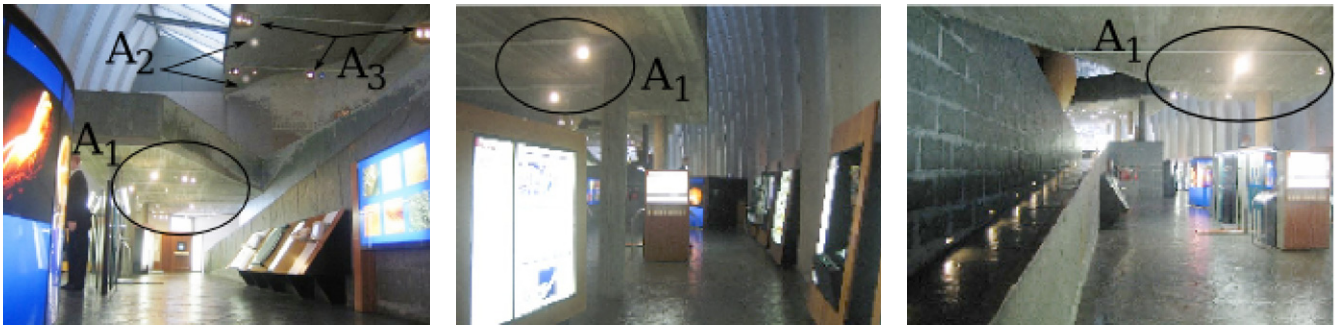

(a) Point of view v_1.

(b) Point of view v_2.

(c) Point of view v_3.

Fig. 7. Snapshots of the environment from different places and points of view (Fig. 6(b)).

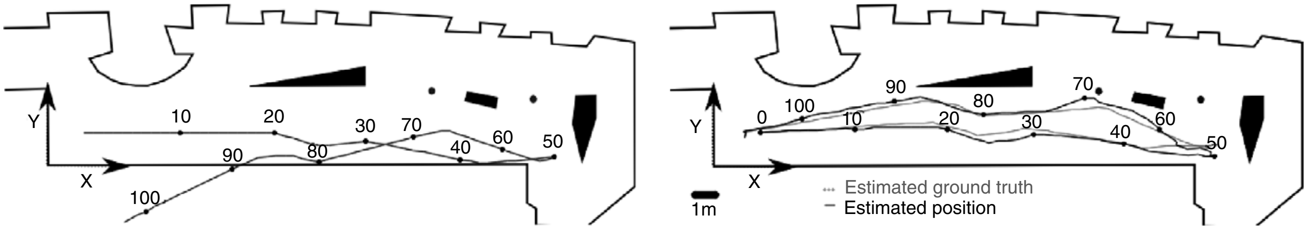

(a) Raw odometry data.

(b) Estimated pose and ground truth.

Fig. 8. Trajectories of the robot for the position tracking experiment.

The position error (Fig. 9(a)) was calculated as the Euclidean distance between the ground truth and the pose obtained by the proposed localization algorithm. The maximum position error in the experiment was 0.75 m and the average error was of 0.29 m. Although the maximum orientation error was of 23°, on an average the error was of only 3°. This angular precision is one of the main advantages of using an omnidirectional camera for localization. The uneven floor of the museum affects the position error very negatively. Nevertheless, the localization system calculates the pose of the robot in a complex environment and over long trajectories with a high degree of precision for navigation tasks.

Fig. 9(d) shows the adaptation of the sample set size through KLD-sampling. We initialized the sample set with 3000 samples generated from a Gaussian distribution centered at the starting pose of the robot. In the first steps, the sample set size quickly decreases to less than 100 samples due to a low localization error. However, when quality of the sample distribution decreases, the number of samples increases up to 1000 samples. This happened, for example, when the robot executed fast turns. This results in a very efficient implementation of the MCL algorithm, as the sample set size (and, therefore, the running time) depends on the quality of the PDF. The running time of the algorithm can be seen in Fig. 9(c). We have used a Intel Pentium 4 CPU 3.06 GHz. The time for processing each image (vision time) was almost constant, except when an image was saturated. In such cases, a second landmark detection process was launched with a higher threshold (see Section 4.1).

5.2. Global localization

The next experiment was performed to show the system's global localization ability. The sample set was initialized with 3000 uniformly distributed samples. Fig. 10 shows the trajectory estimated by the localization algorithm. As can be seen, after a few steps the system determines the position of the robot, and reliably keeps track of it afterward. As we are using the sample-weighted average to estimate the robot's pose, at the beginning the estimated position is always close to the center of the map.

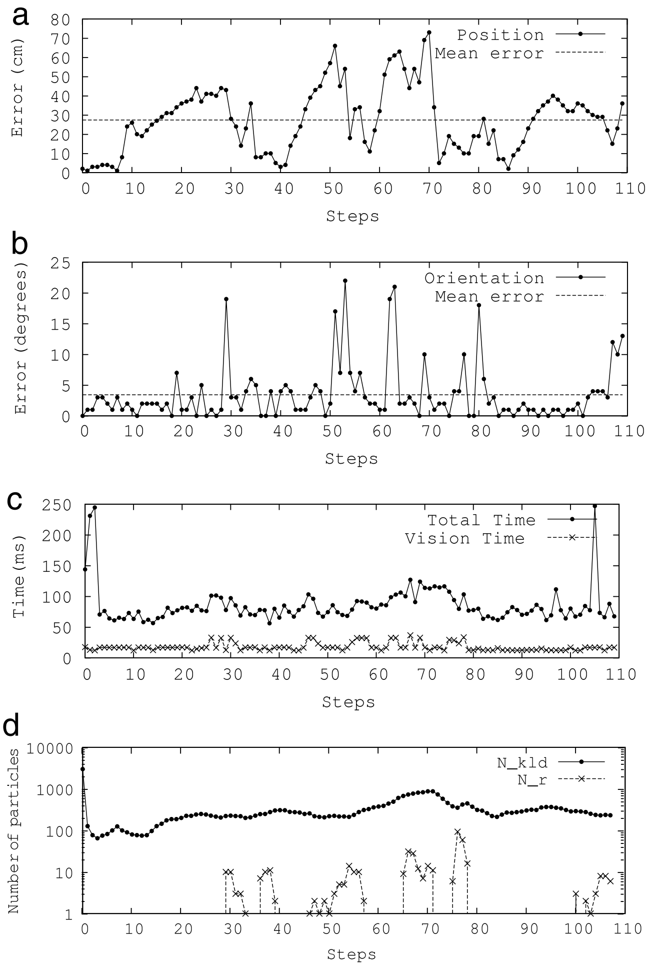

Fig. 9. Results of the position tracking experiment.

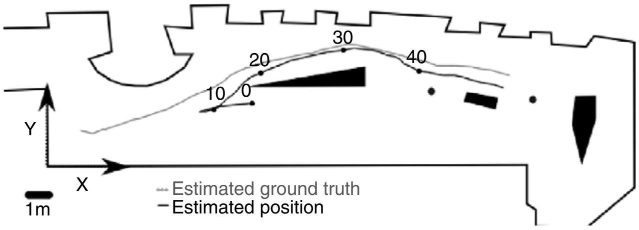

Fig. 10. Trajectory for global localization.

Fig. 11 shows how the sample set converges during the global localization process. The true pose is represented with a square, the estimated pose with a circle, and the samples with points. Samples with the best weights are represented by darker points. At the beginning, samples are randomly distributed over the environment. At each step, the samples progressively converge to the true pose of the robot. It must be noted that, as can be seen in Fig. 11(b) and (c), our environment has symmetries which result in multimodal beliefs. For this reason, our algorithm requires approximately 12–15 steps to converge (Fig. 11(d)) to the correct position of the robot. Nevertheless, the system typically needs only two to three steps to converge to the correct robot's orientation.

Fig. 12 shows the errors in position and angle, the processing time and the number of particles at each step. It can be seen that, at the beginning, the error in position is high and, therefore, the number of particles is also high, thus increasing the processing times. When the robot is localized, all the values are reduced and the problem becomes a position tracking situation.

5.3. Kidnapped robot problem

The third group of experiments was carried out to demonstrate that our system is able to recover from failures. The sample set was initialized as in the previously described position tracking experiment. After integrating 30 images, we provided the localization system with data corresponding to a completely different location. This is equivalent to kidnapping the robot and taking it to a different place in the environment.

The estimated trajectory and pose error of the experiment are shown in Figs. 13 and 14(a) and (b). In these figures the kidnapping situation can be clearly appreciated: there is a sharp increase both in the position and orientation errors at step 30, as the robot was placed in a completely different position. As in the global localization experiment, the system only requires 12–14 steps after kidnapping to recover the position, and two to three steps to obtain the correct orientation.

Similarly, to the position tracking experiment, the sample set size, calculated through KLD-sampling, quickly decreased in the first iteration and then slowly increased due to the symmetries of the environment. When kidnapping was performed, the sample's weights were reduced and the number of random samples (N_r) increased (Fig. 14(d)). At that point, the behavior of the sample set size was similar to the global localization experiment. Initially, the size was increased until the correct position and orientation of the robot were reached and, then, the size was reduced. We repeated this type of experiment with different trajectories and in all the cases the localization system was able to recover from the failure.

5.4. Occlusions

The localization algorithm has been designed to operate under severe and continuous occlusions. A typical situation for this kind of occlusions is when the robot is moving but completely surrounded by people for a long period. Under these conditions, localization methods based on laser range finders fail. Our approach tries to remedy this problem by using an omnidirectional camera and a map of landmarks placed on the ceiling of the environment. However, under these conditions there are still occlusions when the people surrounding the robot being taller than the camera.

We have designed a set of experiments to analyze the performance of KLD-Augmented-MCL under different occlusion conditions. The experiments have been run for the path shown in Fig. 8(b). Occlusions have been artificially generated superposing a mask on the captured images.

The first set of experiments was designed to analyze the performance of the algorithm under continuous occlusions with different degrees. Two types of masks were used: sector (Fig. 15(a)) and ring (Fig. 15(b)). The average error in position and angle along the trajectory are shown in Fig. 16. With the ring mask, both the errors in position and angle for a degree of continuous occlusion of up to a 50% are similar to those of a non-occlusion situation. For the sector mask the same occurs, but up to a degree of continuous occlusion of 40%. Both types of occlusions (but especially the sector occlusion) are highly challenging for the data association, particularly as these occlusions are continuous.

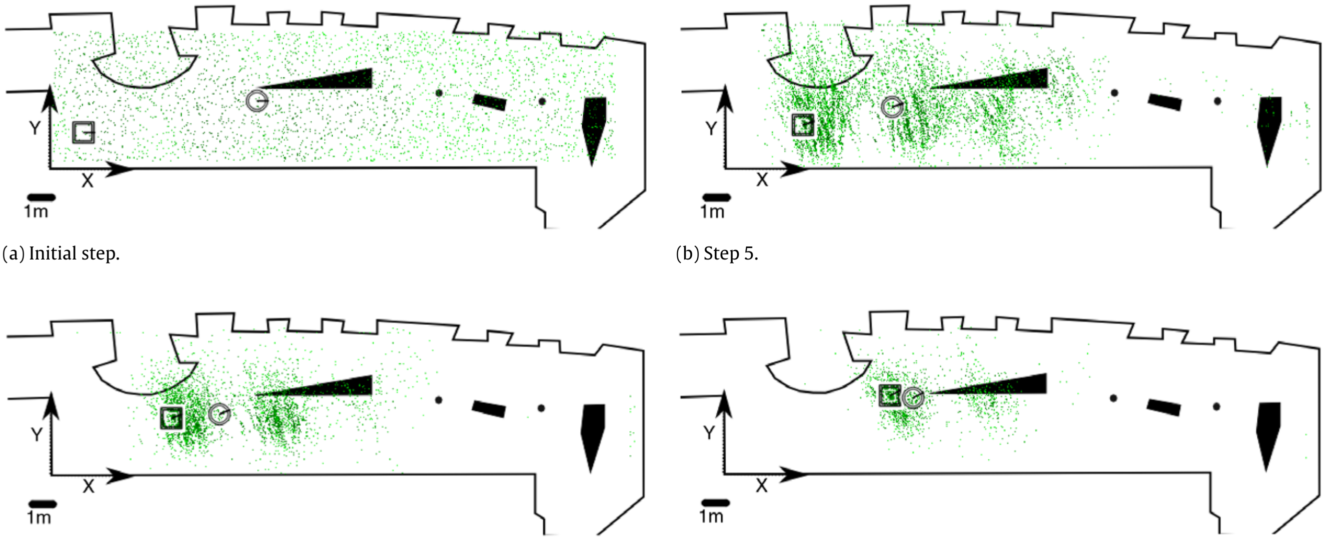

(a) Initial step.

(b) Step 5.

(c) Step 10.

(d) Step 15.

Fig. 11. Sample sets during the global localization experiment.

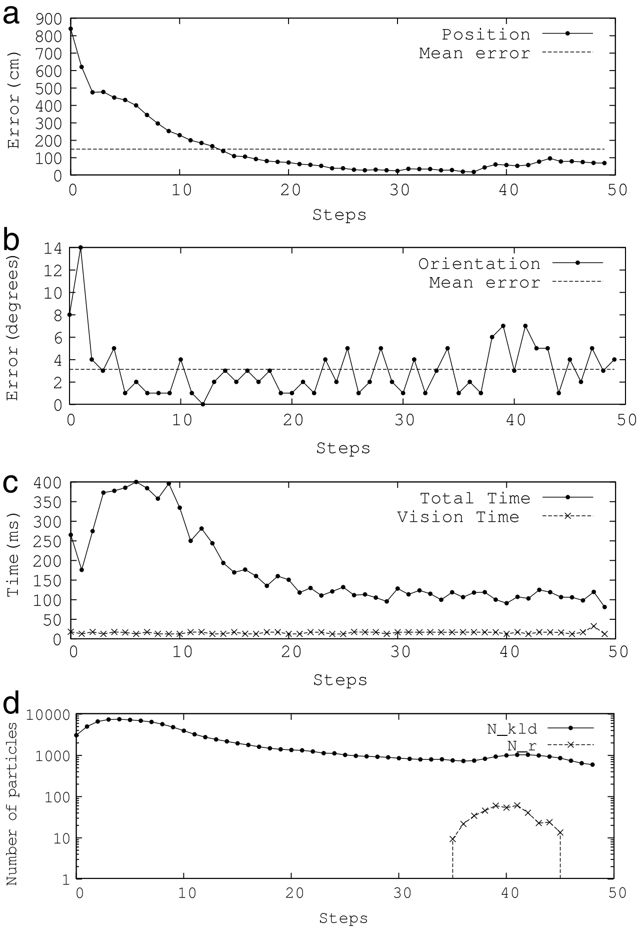

Fig. 12. Results of the global localization experiment.

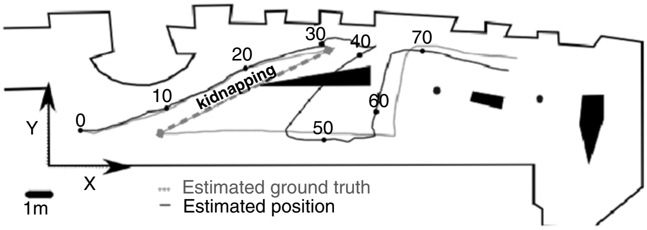

Fig. 13. Trajectory for the kidnapped robot experiment.

The second set of experiments was conducted to analyze the robustness under scattered total occlusions. These occlusions were generated periodically along the trajectory. Fig. 17 shows the average errors in position and angle for different values of the period. It should be noticed that a total occlusion means that all the particles get a very low weight in that iteration (none landmarks are detected). Thus, if total occlusions are very frequent, the sampling process becomes totally random and, therefore, the best particles could disappear. The algorithm shows a great performance for total occlusions of each seven steps (or higher). Under this threshold, the performance decreases, as the particle set is not able to recover from the occlusions.

6. Conclusions

A KLD-Augmented-MCL algorithm based on omnivision has been presented. The system uses a feature-based map of the environment and is able to localize the robot by extracting a list of features from the present omnidirectional image using a camera model. The algorithm works in real-time, as the number of particles is adaptable and the measurement model is scalable with the size of the environment. Moreover, the algorithm is robust to occlusions and changes in the environment.

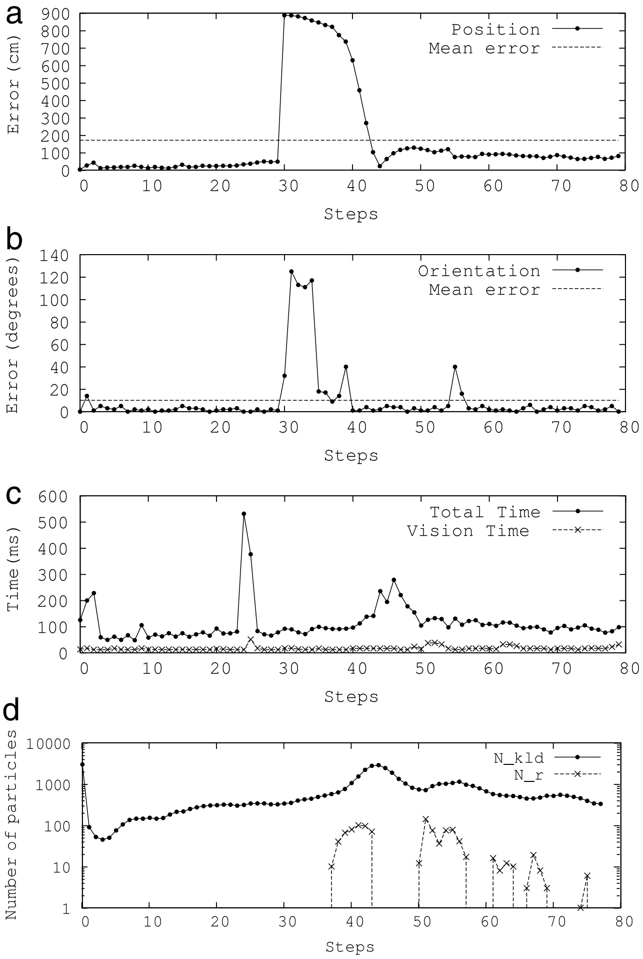

Fig. 14. Results of the kidnapped robot experiment.

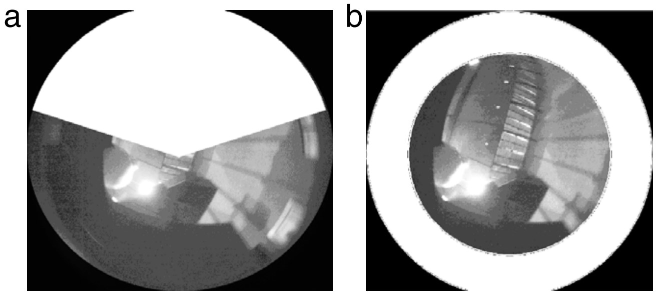

A sector mask.

A ring mask.

Fig. 15. Types of masks used in the continuous occlusion experiments.

The system has been tested on a *Pioneer 2-AT* in a museum environment for position tracking, global localization and the kidnapped robot problem. A deep analysis of the experiments was performed, including the comparison of the estimated trajectory and the estimated ground truth, the position and orientation errors, the processing times, and the number of particles. All the experiments and the analyzed values reflected the proposed localization algorithm's first-rate performance. Moreover, a set of experiments were conducted to show the performance of the algorithm under severe and continuous occlusions. The results demon-

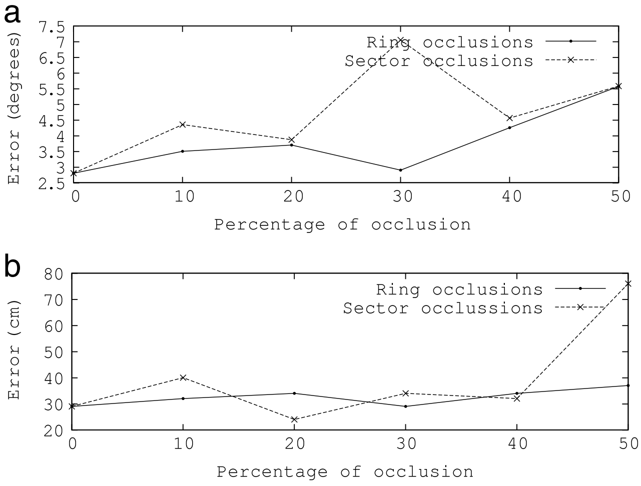

Fig. 16. Errors under continuous occlusions.

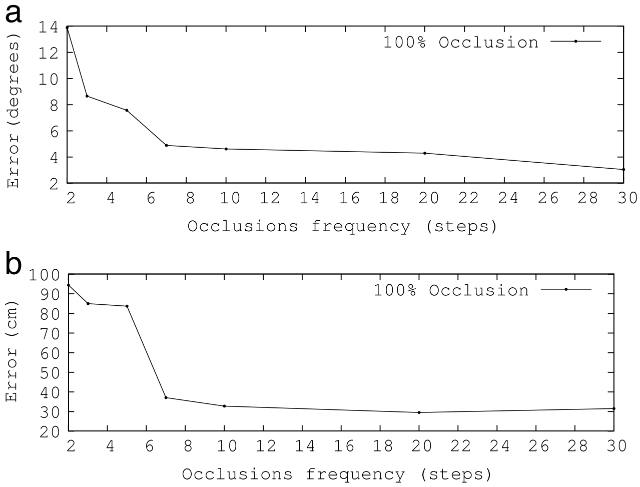

Fig. 17. Errors under periodic total occlusions.

strate that the algorithm is able to correctly localize the robot under real conditions in highly populated environments.

References

[1] S. Thrun, M. Beetz, M. Bennewitz, A. Cremers, F. Dellaert, D. Fox, D. Hähnel, C. Rosenberg, N. Roy, J. Schulte, D. Schulz, Probabilistic algorithms and the interactive museum tour-guide robot minerva, International Journal of Robotics Research 19 (11) (2000) 972–999.

[2] D. Fox, S. Thrun, W. Burgard, F. Dellaert, Sequential Monte Carlo Methods in Practice, Statistics for Engineering and Information Science, Springer, 2001, Ch. Particle Filters for Mobile Robot Localization, pp. 401–428.

[3] J. Leonard, H. Durrant-Whyte, Mobile robot localization by tracking geometric beacons, IEEE Transactions on Robotics and Automation 7 (3) (1991) 376–382.

[4] J. Tardós, J. Neira, P. Newman, J. Leonard, Robust mapping and localization in indoor environments using sonar data, The International Journal of Robotics Research 21 (2002) 311–330.

[5] J. Roda, J. Sáez, F. Escolano, Ceiling mosaics through information-based SLAM, in: Proceedings of the IEEE/RSJ International Conference on Intelligent Robots and System, IROS, San Diego, CA, USA, 2007, pp. 3898–3904.

[6] E. Menegatti, A. Pretto, A. Scarpa, E. Pagello, Omnidirectional vision scan matching for robot localization in dynamic environments, IEEE Transactions on Robotics 22 (3) (2006) 523–535.

[7] S. Thrun, D. Fox, W. Burgard, F. Dellaert, Robust Monte Carlo localization for mobile robots, Artificial Intelligence 128 (1–2) (2001) 99–141.

[8] J.-S. Gutmann, D. Fox, An experimental comparison of localization methods continued, in: Proceedings of the IEEE/RSJ International Conference on Intelligent Robots and System, IROS, Lausanne, Switzerland, 2002, pp. 454–459.

[9] D. Fox, Adapting the sample size in particle filters through KLD-sampling, International Journal of Robotics Research 22 (2003) 985–1003.

[10] D. Chekhlov, M. Pupilli, W. Mayol, A. Calway, Robust real-time visual SLAM using scale prediction and exemplar based feature description, in: Proceedings of the IEEE Conference on Computer Vision and Pattern Recognition, CVPR, Minneapolis, MN, USA, 2007, pp. 1–7.

[11] Y. Sun, Q. Cao, W. Chen, An object tracking and global localization method using omnidirectional vision system, in: Proceedings of the 5th World Congress on Intelligent Control and Automation, Hangzhou, China, 2004, pp. 4730–4735.

[12] H. Andreasson, A. Treptow, T. Duckett, Localization for mobile robots using panoramic vision, local features and particle filter, in: Proceedings of the 2005 IEEE International Conference on Robotics and Automation, ICRA, Barcelona, Spain, 2005, pp. 3348–3353.

[13] M. Mucientes, A. Bugarín, People detection with quantified fuzzy temporal rules, Pattern Recognition, doi:10.1016/j.patcog.2009.11.008.

[14] Z. Zivkovic, B. Kröse, Part based people detection using 2D range data and images, in: Proceedings of IEEE/RSJ Internatlonal Conference on Intelligent Robots and Systems, IROS, San Diego, USA, 2007, pp. 214–219.

[15] D. Hähnel, D. Schulz, W. Burgard, Mobile robot mapping in populated environments, Advanced Robotics 17 (7) (2003) 579–598.

[16] S. Thrun, W. Burgard, D. Fox, Probabilistic Robotics, The MIT Press, 2005.

[17] F. Dellaert, W. Burgard, D. Fox, S. Thrun, Using the CONDENSATION algorithm for robust, vision-based mobile robot localization, in: Proceedings of the IEEE Computer Society Conference on Computer Vision and Pattern Recognition, CVPR, 1999.

[18] M. Moreira, H. Machado, C. Mendonça, G. Pereira, Mobile robot outdoor localization using planar beacons and visual improved odometry, in: Proceedings of the IEEE/RSJ International Conference on Intelligent Robots and Systems, IROS, 2007, pp. 2468–2473.

[19] J. Wolf, W. Burgard, H. Burkhardt, Robust vision-based localization by combining an image retrieval system with Monte Carlo localization, IEEE Transactions on Robotics 21 (2) (2005) 208–216.

[20] Z. Cao, S. Oh, E. Hall, Dynamic omnidirectional vision for mobile robots, Journal of Robotic Systems 3 (1986) 5–17.

[21] A.C. Murillo, C. Sagüés, J. Guerrero, T. Goedemé, T. Tuytelaars, L. Van Gool, Hierarchical localization by matching vertical lines in omnidirectional images, in: Proceedings of the First From Sensors to Human Spatial Concepts Workshop, 2006, pp. 13–19.

[22] A. Koenig, S. Mueller, H.-M. Gross, Appearance-based CML approach for a home store environment, in: Proceedings of the 2nd European Conference on Mobile Robots, ECMR, 2005, pp. 206–211.

[23] E. Brassart, L. Delahoche, C. Cauchois, C. Drocourt, C. Pegard, E. Mouaddib, Experimental results got with the omnidirectional vision sensor: Syclop, in: Proceedings of the IEEE Workshop on Omnidirectional Vision, 2000, pp. 145–152.

[24] E. Menegatti, M. Zoccarato, E. Pagello, H. Ishiguro, Image-based Monte-Carlo localisation with omnidirectional images, Robotics and Autonomous Systems 48 (1) (2004) 17–30.

[25] H.-M. Gross, A. Koenig, S. Mueller, Vision-based Monte Carlo self-localization for a mobile service robot acting as shopping assistant in a home store, in: Proceedings of the IEEE/RSJ International Conference on Intelligent Robots and Systems, IROS, 2002, pp. 256–262.

[26] F. Dellaert, D. Fox, W. Burgard, S. Thrun, Monte Carlo localization for mobile robots, in: Proceedings of the International Conference on Robotics and Automation, ICRA, Detroit, MI, USA, 1999, pp. 1322–1328.

[27] D. Fox, W. Burgard, F. Dellaert, S. Thrun, Monte Carlo localization: Efficient position estimation for mobile robots, in: Proceedings of the National Conference on Artificial Intelligence, AAAI, Orlando, FL, USA, 1999, pp. 343–349.

[28] H. Bakstein, T. Pajdla, Panoramic mosaicing with a 180° field of view lens, in: Proceedings of the Third Workshop on Omnidirectional Vision, 2002, pp. 60–67.

C. Gamallo received the Technical Engineering degree and the M.Sc. degree in Computer Science at the University of A Coruña, Spain, in 2002 and 2006, respectively. She is presently a Ph.D. Student in the Department of Electronics and Computer Science, University of Santiago de Compostela, Spain. Her present research interests include image processing (specially for mobile robotics), robotics localization and visual Simultaneous Localization and Mapping (SLAM).

C.V. Regueiro received the B.S. and Ph.D. degrees in Physics from the University of Santiago de Compostela, Spain, in 1992 and 2002, respectively. Since December 1993, he has been an Associated Professor in the Faculty of Computer Science at the University of A Coruña, Spain, where he teaches undergraduates and graduates courses on computer architecture. His research interests focus on control architectures, perception, control, localization, navigation and machine learning in mobile robotics.

P. Quíntia received the M.Sc. degree in Computer Science at the University of A Coruña, Spain, in 2007. He is presently a Ph.D. Student in the Department of Electronics and Computer Science, University of Santiago de Compostela, Spain. His research is focused on image processing, artificial neural networks, reinforcement learning and their applications in mobile robotics.

M. Mucientes received the M.Sc. and Ph.D. Degrees in Physics from the University of Santiago de Compostela, Spain, in 1997 and 2002, respectively. He is presently a *Ramón y Cajal* research fellow with the Department of Electronics and Computer Science, University of Santiago de Compostela. His present research interests include evolutionary algorithms, genetic fuzzy systems (specially for mobile robotics), visual Simultaneous Localization and Mapping (SLAM), spatio-temporal pattern recognition, and multitarget-multisensor tracking.